CHEMISTRY
AN ASIAN JOURNAL

DOI: 10.1002/asia.200600014

Transition States of Binap–Rhodium(I)-Catalyzed Asymmetric Hydrogenation: Theoretical Studies on the Origin of the Enantioselectivity

Seiji Mori,*[a, b] Thom Vreven,[b, c] and Keiji Morokuma*[b]

Abstract: By using the hybrid IMOMM(B3LYP:MM3) method, we examined the binap–Rh^{I}-catalyzed oxidative-addition and insertion steps of the asymmetric hydrogenation of the enamide 2-acetylamino-3-phenylacrylic acid. We report a path that is energetically more favorable for the major enantiomer than for the minor enantiomer. This path follows the "lock-and-key" motif and leads to the major enantiomeric product via an energetically favorable binap–dihydride–Rh^{III}–enamide complex. Our theoretical results are consistent with the mechanism that takes place via Rh^{III} dihydride formation, that is, oxidative addition of H_2 followed by enamide insertion.

Keywords: asymmetric hydrogenation · chiral ligands · density functional calculations · enantioselectivity · rhodium

Introduction

The catalytic asymmetric hydrogenation of alkenes is one of the most successful methods in asymmetric synthesis; its discoverers were awarded the 2001 Nobel prize in chemistry.[1–4] The ligand–Rh^{I}-catalyzed reactions of α-acetamidocinnamic acid and its derivatives are highly enantioselective, as shown in Equation (1) for a number of chiral ligands.[5] In particular, Noyori and co-workers reported excellent enantioselectivity (>90% *ee*, *S*) with an (*R*)-binap ligand.[3]

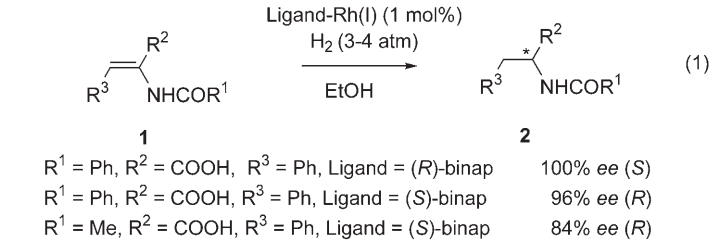

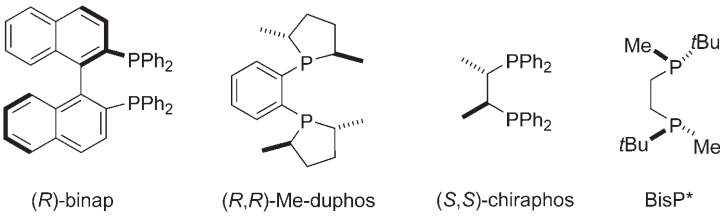

Despite numerous efforts to elucidate the high enantioselectivity, the reaction mechanisms and the origin of the stereoselectivity are still important subjects of research.[6] Two mechanisms have been proposed in the literature. First, the unsaturated (Path A in Scheme 1) or Halpern–Landis–Brown mechanism involves an initial chelate formation between a chiral Rh catalyst and the enamide, followed by the oxidative addition of H_2.[7–10] Second, in the dihydride mechanism, a rhodium dihydride is formed, followed by coordination of the alkene in a bidentate phosphine molecule.[11]

The unsaturated mechanism is strongly supported by X-ray crystal structures,[12,13] CD analyses,[14] and kinetic and binding constants between the Rh catalyst and enamide from NMR and UV/Vis spectroscopy.[15–18] The hydrogenation reaction mechanisms of enamides with a Me-duphos ligand have been examined both experimentally[7] and theoretically.[19–22b] The "anti-lock-and-key" motif was proposed, in which the major enantiomer is produced through the less-

[a] Prof. S. Mori
Faculty of Science, Ibaraki University
Bunkyo, Mito 310-8512 (Japan)
Fax: (+81) 29-228-8403
E-mail: smori@mx.ibaraki.ac.jp

[b] Prof. S. Mori, Dr. T. Vreven, Prof. K. Morokuma
Cherry L. Emerson Center for Scientific Computation and
Department of Chemistry, Emory University
Atlanta, GA 30322 (USA)
Fax: (+1) 404-727-7412
E-mail: morokuma@emory.edu

[c] Dr. T. Vreven
Gaussian, Inc.
340 Quinnipiac St. Bldg 40, Wallingford, CT 06492 (USA)

Supporting information for this article is available on the WWW under http://www.chemasianj.org or from the author.

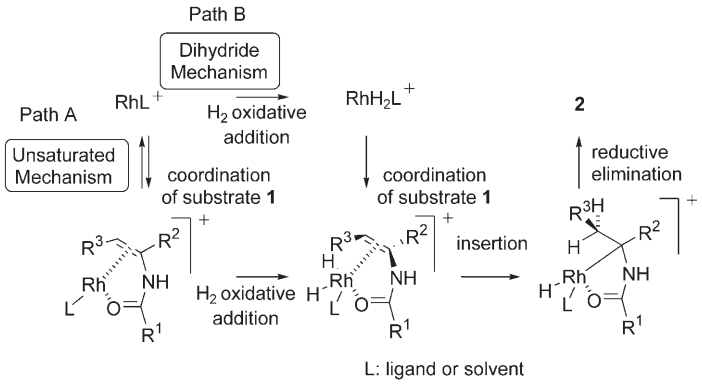

Scheme 1. Conventional mechanisms of Rh(I)-catalyzed hydrogenation.

stable of two diastereomeric catalyst–enamide complexes followed by the more-stable diastereomeric transition states of the oxidative-addition or insertion steps.[10,18,20–22,30] Several potential pathways (Paths 1–4 in Scheme 2) in the unsaturated mechanism have been identified by Landis and Feldgus in the reaction of $CH_2=CR^2(NHCHO)$ ($R^2=CN$, *t*Bu) with a Me-duphos catalyst through careful ONIOM-(B3LYP:UFF) analyses,[22a,b,23] followed by recent B3LYP studies on the reaction of $CH_2=CR^2(NHCHO)$ ($R^2=CN$) with a BisP* catalyst.[22c] However, in their studies, the 3-phenyl and carboxy groups at the enamide were substituted by H and CN, respectively. As shown in Scheme 2, Path 1 involves the formation of the weakly bound five-coordinated molecular-hydrogen complex **4** from a four-coordinated complex **3**, followed by oxidative addition to give the six-coordinated Rh^{III} dihydride complex **5** and subsequent Rh–H insertion to give a Rh^{III} α-alkyl hydride intermediate **6**. The coordination geometry of the nearly square planar **3** is similar to the crystal structure of the [Rh(chiraphos)(ethyl (*Z*)-α-acetamidocinnamate)] complex, in which the phosphine ligand occupies a position *trans* to the amide carbonyl moiety of the enamide.[12,24] In **5**, one hydride occupies the *trans* position relative to the C=C bond. Path 2 involves the formation of the six-coordinated Rh dihydride complex **8** through the weakly bound five-coordinated molecular-hydrogen complex **7**. In **7**, the hydrogen molecule occupies a position *trans* to the amide carbonyl moiety. According to Landis and Feldgus, it is highly unlikely that the reaction proceeds by Path 2 because of the high barrier of formation of **7**.[21] The interconversion between diastereomeric precursor complexes or the isomerization between precursors **4** and **7** for oxidative addition in Paths 1 and 2 is possible according to previous experimental[25] and computational studies. The regioisomeric pathways Paths 3 and 4 were also previously examined. In Path 4, the six-coordinated Rh dihydride intermediate **14** is reached through a channel (**3**→**13**→**14**).

Besides **3**, its coordination isomer **16**, in which two phosphorus, the olefinic carbon, and the Rh atoms lie in the same plane, was examined herein for the first time. The conversion of **16** into the five-coordinated complex **17** has not yet been considered by theory. Complex **17** leads to either **8** or **14** through Path 2′ or 4′, respectively (Scheme 2).

The alternative dihydride mechanism (Path B in Scheme 1) was proposed based on recent kinetics and NMR spectroscopic measurements, specifically with [2.2]phanephos, miniphos–Rh^I, and BisP*–Rh^I catalysts (phanephos = 4,12-bis(diphenylphosphino)-[2.2]-paracyclophane, miniphos = 1,2-bis(alkylmethylphosphino)methane).[26–33] A solvated Rh dihydride complex [RhH_2(BisP*)] was observed, which leads to the hydrogenation product after the addition of enamides.

It is clear that only one of two possible diastereomers of the Rh^I–binap complex with enamide is formed, according to ^{31}P NMR spectroscopic studies (see above).[34] There have hardly been any detailed kinetic studies on Rh^I–binap-catalyzed hydrogenation, whereas such studies with Ru^{II}–binap were recently reported.[35] Recent studies showed that the kinetically controlled diastereoselectivity of H_2 addition to $[Ir(cod)]^+$ complexes (cod = 1,5-cyclooctadiene) with some ligands (chiraphos and norphos; norphos = 5,6-bis(diphenylphosphino)-2-norbornene) does not relate to high enantioselectivity of asymmetric hydrogenation of enamides with $[Rh(diphosphine)]^+$ complexes. On the other hand, the binap–Ir^I or binap(Me-duphos)–Ir^I complexes demonstrate high diastereoselectivity in oxidative addition, and the selectivity does not change with temperatures as with the BisP* ligand.[31,36] Hence, the mechanisms of the hydrogenation re-

Abstract in Japanese:

IMOMM(B3LYP:MM3)法を用い，エナミド，2-アセチルアミノ-3-フェニルアクリル酸の Rh^I-binap 触媒による不斉水素化反応の酸化的付加反応および挿入反応の遷移状態を求めた．注目すべきことは，エネルギー的に多少安定な四配位ロジウムーエナミド錯体から主エナンチオマーが生じることであり，この反応は「鍵—穴」原理にもとづく．最も安定な経路上の，酸化的付加および挿入反応の遷移状態のエネルギーをみたところ，主エナンチオマーを生成する経路の方が低かった．

International Advisory Board Member

Keiji Morokuma *is William H. Emerson Professor of Chemistry and the Director of the Emerson Center for Scientific Computation at Emory Univ. From September 1, 2006, he is Professor Emeritus at Emory Univ. and Research Leader at the Fukui Institute for Fundamental Chemistry at Kyoto Univ. He was a professor at the Univ. of Rochester and the Institute for Molecular Science at Okazaki, Japan. He has authored over 580 scientific publications.*

"The 21st century will be the century of Asia, and Chemistry—An Asian Journal *will become one of the most important journals in chemistry."*

CHEMISTRY
AN ASIAN JOURNAL

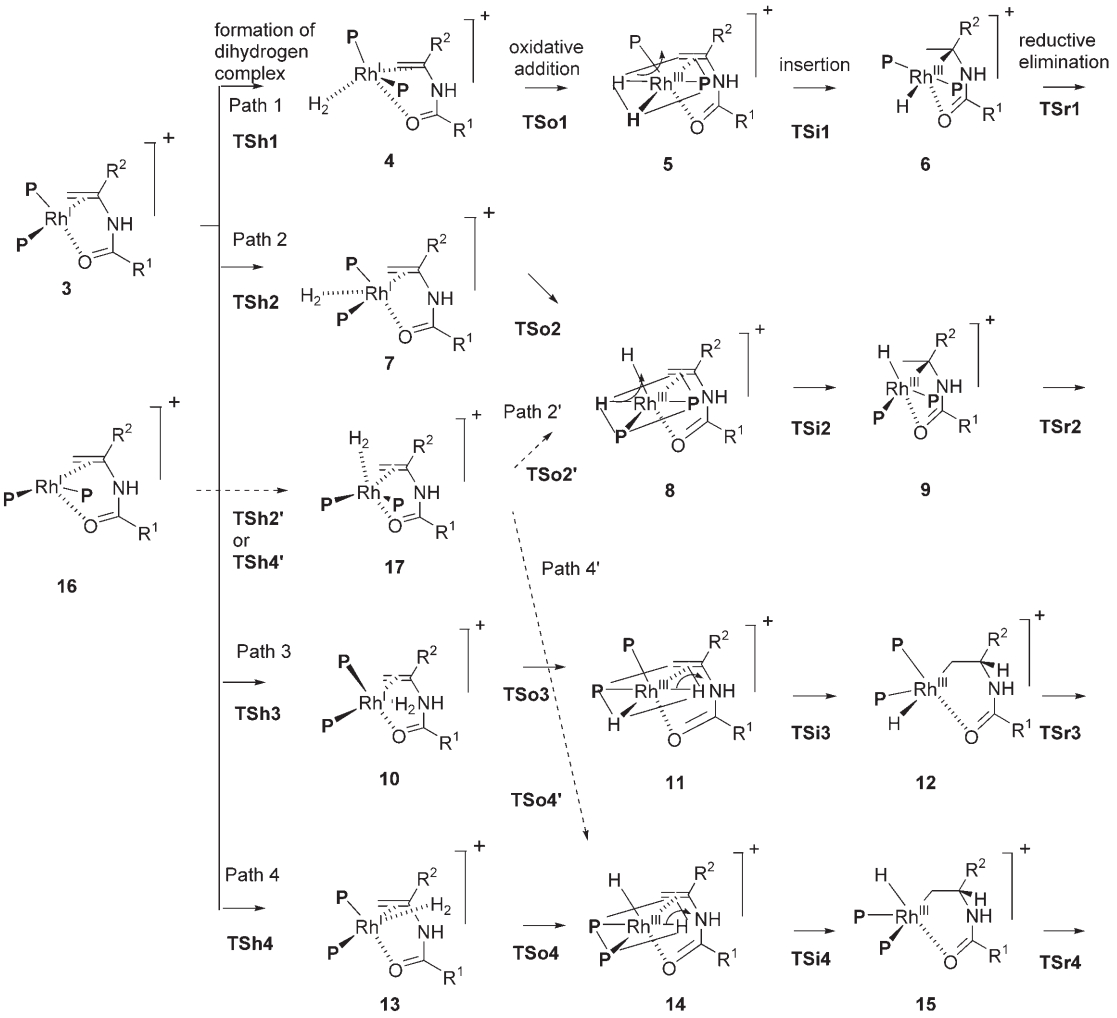

3-alkyl group (R^3 in Scheme 1) of (*E*)-enamide is omitted.
3-alkyl group = H; R^1 = H; R^2 = CN; **P** = PH_3[21]
3-alkyl group = H; R^1 = H; R^2 = CN, *t*Bu; $\mathbf{P_2}$ = Me-duphos[22a]
3-alkyl group = H; R^1 = H; R^2 = CN; $\mathbf{P_2}$ = BisP*[22c]
3-alkyl group = H; R^1 = H; R^2 = COOH;**P** = PH_3 (small model system, present work)
3-alkyl group = Ph; R^1 = Me; R^2 = COOH; $\mathbf{P_2}$ = binap (real model system, present work)

Scheme 2. Reaction pathways for Rh(I)-catalyzed hydrogenation reactions of enamides.

actions with a binap–Rh^I catalyst are still controversial: 1) Which step determines the stereoselectivity in the multistep hydrogenation reaction? 2) Does the "lock-and-key" or the "anti-lock-and-key" motif apply to the hydrogenation reaction of $[Rh(binap)]^+$ with enamides? 3) Does the hydrogenation follow the unsaturated or dihydride mechanism?

Herein we present for the first time the origin of enantioselectivity of the binap–Rh^I-catalyzed asymmetric hydrogenation of enamides, focusing on the transition states for the pathways of the unsaturated mechanism (Paths 1–4, Scheme 2) as well as the new pathways Paths 2′ and 4′. We used $[Rh(PH_3)_2]^+$ with 2-formylaminoacrylic acid as a small model system for preliminary studies, then switched to [Rh(binap)]$^+$ with a β-phenyl-substituted enamide, 2-acetylamino-3-phenylacrylic acid, as a real model system. The coordination isomers involving the oxidative-addition and insertion steps are shown in Scheme 2.[23,37,38] We focused on processes after the formation of the Rh^{III} dihydride/enamide complexes. In the structures of precursor complexes **4**, **7**, **10**, **13**, and **17** for oxidative addition, the Rh atom was found to be chelated due to the coordination ability of the COOH group and the lack of a solvent molecule.

For the small model system, we used the B3LYP density functional method. The B3LYP functional is reliable for investigations of Rh complexes.[39,40] However, the stereoelectronic effects of the phosphine ligands may not be properly described by PH_3 (instead of PPh_2R) in the case of Rh-catalyzed hydroformylation,[41] but the real model system to be examined is too costly with full B3LYP density functional calculations (especially normal mode analyses, which takes

five days with 16 CPUs on the NEC TX-7 computer). Therefore, we used the integrated molecular orbital and molecular mechanics (IMOMM) method, which constitutes a molecular orbital (MO) and a molecular mechanics (MM) part (MM3; Figure 1).[42] The IMOMM method has been used for the investigation of many organometallic reactions,[43] and was later generalized to the ONIOM method, which can combine up to three levels of MO methods as well as an MM.[44] Although the ONIOM method is an improvement over IMOMM in most respects, the MM3 force field[45] used herein is not implemented in the current version of the Gaussian 03 package. As to the reliability of the IMOMM method, a previous study showed that in the reaction with H_2, the diastereomer of [Rh(chiraphos)(PhCH=C(NHC(=O)Me)COOH)]$^+$ that led to the minor enantiomer was 11.1 kJ mol^{-1} lower in energy than the other diastereomer that led to the major enantiomer at the IMOMM(B3LYP/I:MM3(92)) level. This result was consistent with previous experimental studies (see Supporting Information). The IMOMM-optimized structure is also similar to the X-ray crystallographic and SHAKE/CHARMM-optimized structures of [Rh(chiraphos)(PhCH=C(NHC(=O)Me)COOEt)]$^+$.[12,14,24]

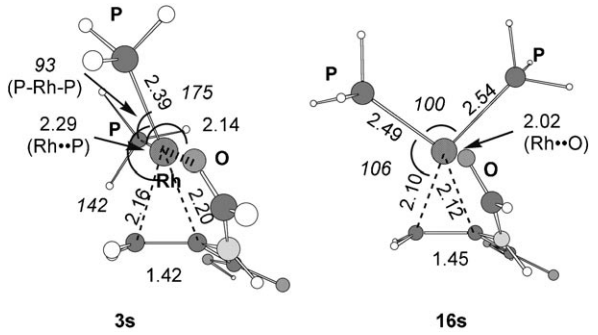

Figure 2. Structures of precursor complexes at the B3LYP/II level. Bond lengths are in Å, bond angles (italics) in degrees.

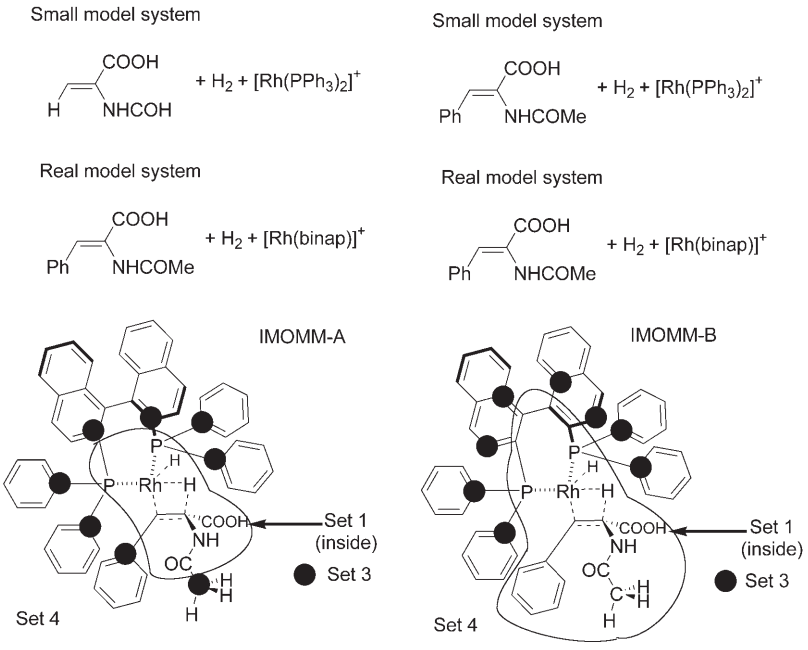

Figure 1. Definition of small and real model systems and sets of atoms in the two IMOMM partitions A and B. (*R*)-binap is shown in the system.

Results and Discussion

Reaction of the Small Model System

First, several reaction pathways (Scheme 2) were examined for the small model system ($[Rh(PH_3)_2]^+ + CH_2=C$(NHCHO)COOH). The structures of the two four-coordinate substrate complexes **3s** and **16s** (s denotes small) are shown in Figure 2. The two complexes are mutually coordinatively isomeric. In **3s**, the rhodium atom has a nearly square arrangement that is common to Rh^{I} complexes, as known from previous X-ray crystallographic[12,24,54] and NMR spectroscopic studies[55] of related Rh complexes. The isomeric complex **16s** has a nearly tetrahedral arrangement and is less stable than **3s** by 120 kJ mol^{-1}.

The transition states (TSs) (**TSh1s**, **TSh2s**, **TSh2′s**, **TSh3s**, **TSh4s**, **TSh4′s**) for the formation of the five-coordinated dihydrogen complexes (**4s**, **7s**, **10s**, **13s**, **17s**), the TSs (**TSo1s**, **TSo2s**, **TSo2′s**, **TSo3s**, **TSo4s**, **TSo4′s**) for the oxidative addition, its resultant intermediates (**5s**, **8s**, **11s**, **14s**), the TSs (**TSi1s**–**TSi4s**) for the alkene insertion into the Rh−H bond, and the resultant rhodium(III) hydride intermediates (**6s**, **9s**, **12s**, **15s**) for Paths 1–4 (Scheme 2) are shown in Figures 3–6. The energetics of the reaction pathways are shown in Figure 7. Paths 1, 2, and 2′ involve a nucleophilic attack of a hydride ion at the less-hindered sp^2 carbon of $CH_2=C$(NHCHO)COOH, whereas regioisomeric Paths 3, 4, and 4′ involve attack at the other disubstituted sp^2 carbon.

Paths 1 and 3 start with a side-on approach of a hydrogen molecule to different sides of the square-planar structure of the lower-energy Rh complex **3s**, giving the transition states for the formation of the five-coordinate dihydrogen complexes, **TSh1s** and **TSh3s**, respectively. The energy of **TSh1s** is higher than that of the reactant **3s** by 9.1 kJ mol^{-1}, whereas the energy of **TSh3s** is lower than that of **3s** by 3.3 kJ mol^{-1} (thus suggesting the existence of an unimportant small energy minimum between **3s** and **TSh3s**). The end-on approach of a hydrogen molecule to **3s** gives directly (with-

CHEMISTRY
AN ASIAN JOURNAL

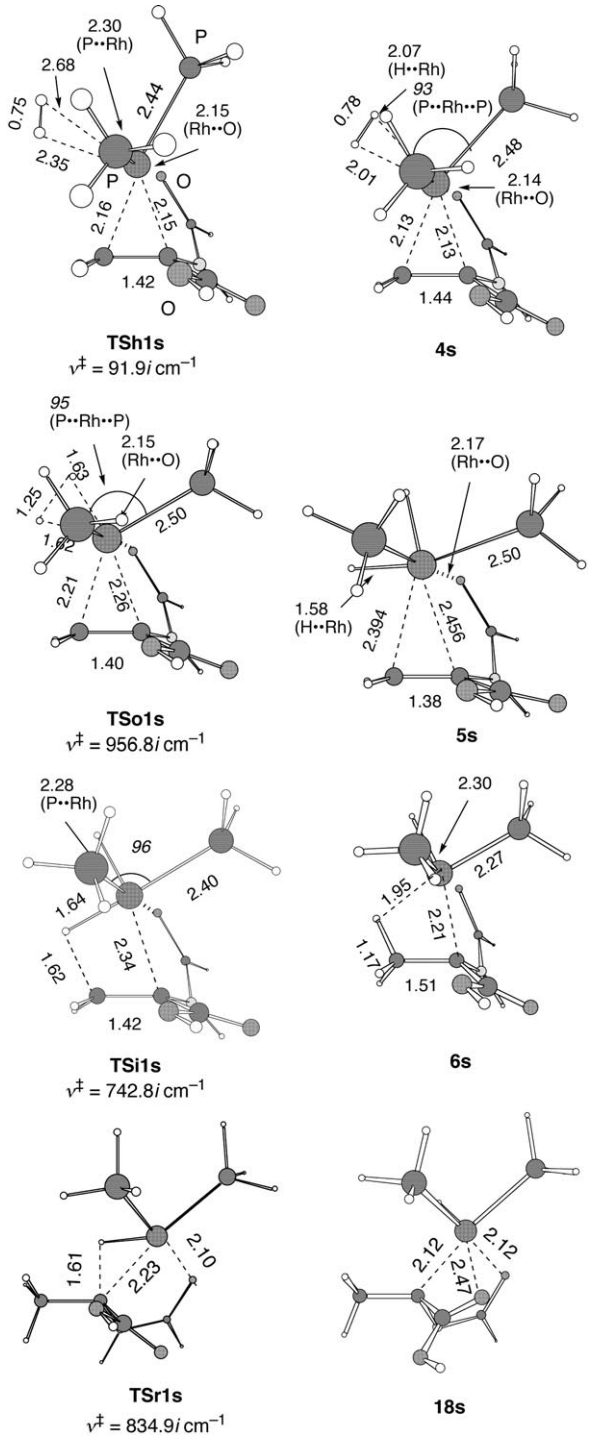

Figure 3. Structures of intermediates and transition states in Path 1 of the small model system at the B3LYP/II level. Bond lengths are in Å, bond angles (italics) in degrees. ν^{+} refers to an imaginary frequency.

out barrier) the dihydrogen complexes **7s** and **13s**, respectively. Optimization of the transition states for formation of five-coordinated dihydrogen complexes for the higher-energy Rh complex **16s** from different directions (Paths 2′ and 4′) gives a single structure **TSh2′s/TSh4′s**. The coordination geometry of this transition state **TSh2′s** is similar to that of **16s**, which is reflected by the small energy difference of 3.2 kJ mol^{-1}. **TSh2′s/TSh4′s** gives **17s**, during which the dissociating H–H bond is stretched to 0.83 Å; **17s** is 39.8 kJ mol^{-1} less stable than **3s**. The reactant **3s** and these weakly bound dihydrogen complexes are connected with low or no barriers and are likely to be in equilibrium.

For the oxidative-addition reaction that maintains the π coordination between the rhodium atom and the alkene of the enamide, we found six TSs corresponding to six dihydrogen complexes. **TSo1s** in Path 1 is 16 kJ mol^{-1} lower in energy than **TSo2′s** in Path 2′. For Path 2′, **TSo2′s** from the less-stable **17s** is lower in energy by 27 kJ mol^{-1} than **TSo2s** from the more-stable **8s**. Intrinsic reaction path (IRC) calculations showed that both **TSo2s** and **TSo2′s** lead to **8s**. Similarly for Paths 3 and 4′, **TSo3s** is more stable by 14.4 kJ mol^{-1} than **TSo4′s** from less-stable **17s** in Path 4′; **TSo4′s** is in turn 23.8 kJ mol^{-1} lower in energy than **TSo4s** from the more-stable **13s**. Both **TSo4s** and **TSo4′s** lead to **14s**.

In the enamide insertion step, **TSi1s** is higher in energy than **TSi2s** by as much as 36.3 kJ mol^{-1}. The activation energy of the insertion step (**8s** to **TSi2s** in Path 2) of 2.6 kJ mol^{-1} is small and is comparable to the 0.9 kJ mol^{-1} in the insertion to $CH_2=C(NHCHO)CN$.[19] The transition state in Path 3 (**TSi3s**) of 98.4 kJ mol^{-1} is very high in energy. The insertion transition states **TSi1s**, **TSi2s**, **TSi3s**, and **TSi4s** lead to alkylrhodium intermediates **6s**, **9s**, **12s**, and **15s**, respectively. The agostic interactions have been observed both experimentally and theoretically in **6s** and **9s**.[32,56] In the isomerization pathways from **6s** or **9s** with agostic interactions to the intermediates **18s** or **19s**, we were only able to locate the transition state in Path 2 (**TSag2s**); the optimization of the TS (**TSag1s**) in Path 1 failed. The activation energy from **9s** to **TSag2s** is 114.2 kJ mol^{-1} (Figure 7). The energy of the transition state of reductive elimination, **TSr2s**, is also high. Although we did not follow this step of the reaction carefully, solvent effects of methanol may have lowered the barrier and facilitated the pathway.

Overall, Paths 1 and 2 are favorable over regioisomeric Paths 3 and 4, respectively. The formation of the weakly bound Rh–H_2 complex **17s** from **16s** is highly unfavorable.

Isomerization Process between Paths 1 and 2

The transition states for the dihydride isomerization process that connects Paths 1 and 2 in the $[Rh^{I}(PH_3)_2]^{+}$ complex with α-acetamidoacrylonitrile were previously examined.[21] The rate-determining TS for isomerization (**TS12s**) between Rh^{III} dihydride complexes **5s** and **8s** was optimized for the present model, and is shown in Figure 8. **TS12s** is higher in energy than the TS for dihydrogen oxidative addition for Path 1, **TSo1s**, but is slightly lower in energy than **TSo2s** and **TSo2′s** in Path 2. Hence, this isomerization of the small model system may occur as well as a rapid equilibrium between the Rh^{III} dihydride complexes and the reactant. In the real model system, with bulky chiral ligands and solvent

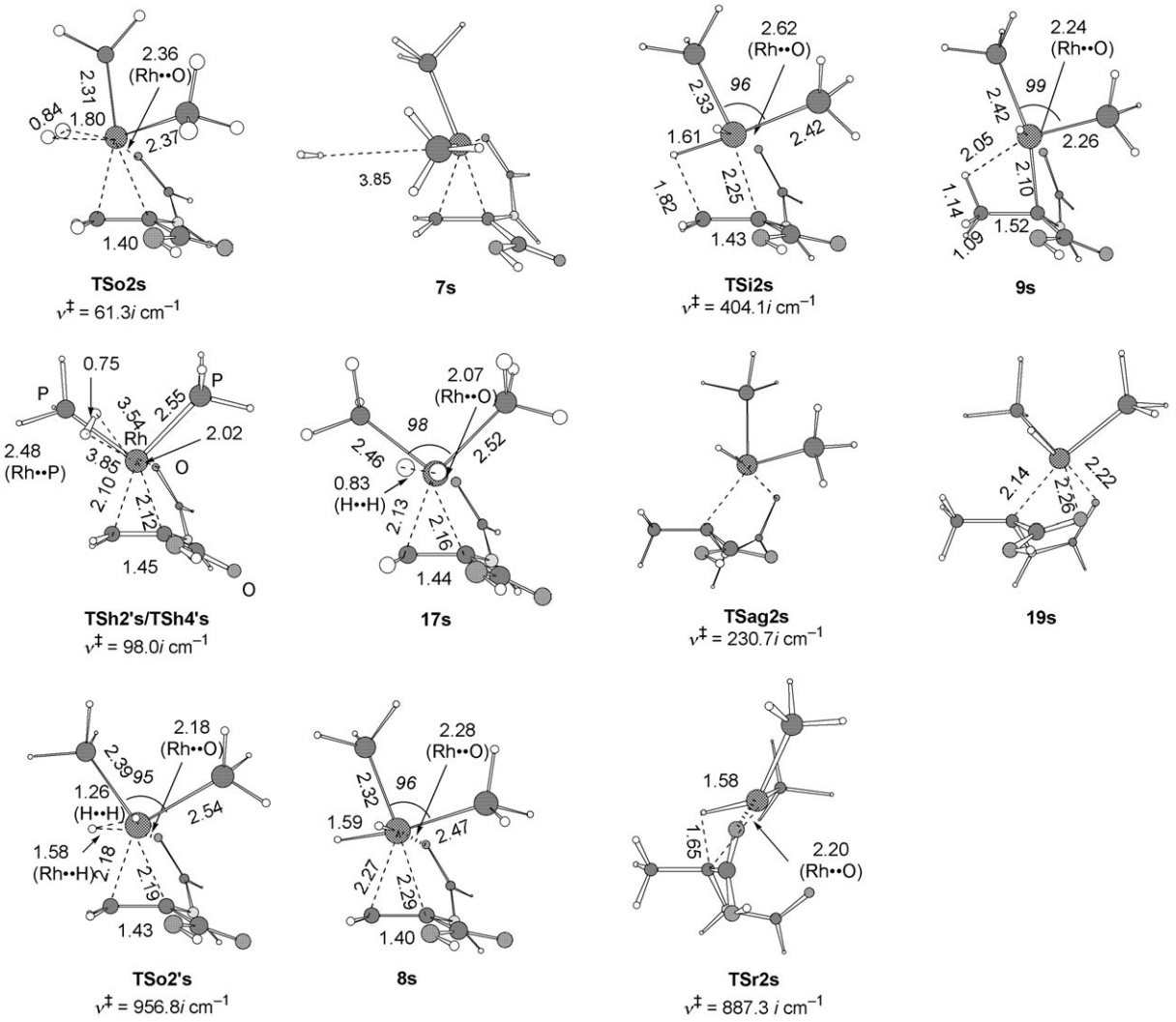

Figure 4. Structures of intermediates and transition states in Path 2 of the small model system at the B3LYP/II level. Bond lengths are in Å, bond angles (italics) in degrees.

molecules, such an isomerization would not be possible and will be excluded from explicit consideration.

Reaction of the Real Model System

With the above results in mind, we now employed the IMOMM method to examine the effects of bulky substituents in the real model system on various transition states. The ligation of a binap–Rh^{I} catalyst to enamide gives four diastereomers of four-coordinate Rh^{I} complexes, **3M**, **3m**, **16M,** and **16m**. M is used for stationary points on the pathway that lead to a major product enantiomer, and m for those on the pathway that leads to a minor enantiomer. The complex leading to the major product **3M** is 15.8 kJ mol^{-1} more stable than the complex leading to the minor product **3m** at the IMOMM-BII level with IMOMM-AI-optimized geometries (3.0 kJ mol^{-1} more stable at the B3LYP/II level; Figure 9). The energetics of the COOH group rotamers do not change very much. The fact that the major **3M** is slightly lower in energy the minor **3m** complex is opposite to the cases of duphos and chiraphos.[34] The optimized structures of **16M** and **16m** at the IMOMM-AI level have very high energy, and reoptimization of these structures at the IMOMM-BII level converged to **3M** and **3m**. We can conclude that **16M** and **16m** are high in energy if they exist. We also obtained five-coordinate dihydrogen complexes **7M** and **7m**, but could not find any complex **4** corresponding to the approach of dihydrogen from the other direction.

Paths 1, 2, and 2′

We first studied the transition states in Path 1 (Figure 10). The TS of oxidative addition of dihydrogen in the major pathway, **TSo1M**, is 6.4 kJ mol^{-1} lower in energy than that in the minor pathway, **TSo1m**. The transition state of alkene insertion to give the major enantiomer, **TSi1M**, is also more stable than the minor TS, **TSi1m**, by 4.6 kJ mol^{-1}. Thus, the energetics of both oxidative addition and alkene insertion in Path 1 are consistent with the experimental enantioselectivi-

CHEMISTRY
AN ASIAN JOURNAL

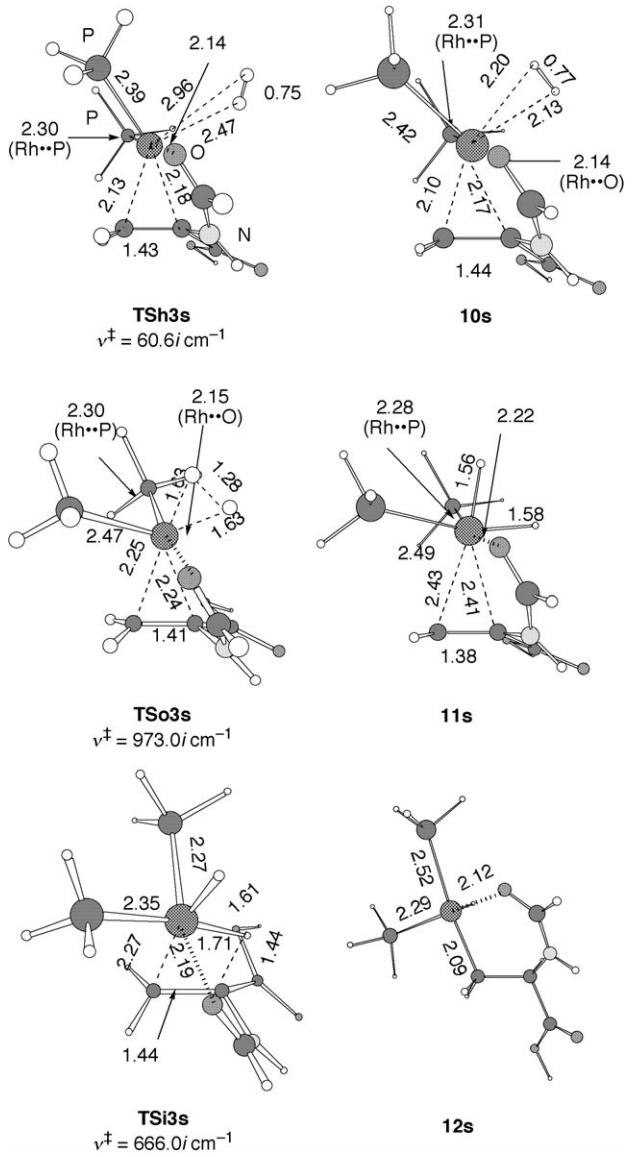

Figure 5. Structures of intermediates and transition states in Path 3 of the small model system at the B3LYP/II level. Bond lengths are in Å, bond angles (italics) in degrees.

Figure 6. Structures of intermediates and transition states in Path 4 of the small model system at the B3LYP/BAS-II level. Bond lengths are in Å, bond angles (italics) in degrees.

ty (84 % *ee*, corresponding to the Gibbs energy difference of 4.5 kJ mol^{-1} at 298 K). If the enantioselective hydrogenation occurs through Path 1, the oxidative-addition step (with higher TS energy than the insertion step) should be rate-determining and is likely to make a larger contribution to the enantioselectivity than the insertion step (with the **m**-**M** energy difference of 6.4 kJ mol^{-1} at the oxidative-addition vs. 4.6 kJ mol^{-1} at the insertion TS), although the **m**-**M** energy difference is too small for quantitative comparison.

To clarify the origin of the enantioselectivity, the IMOMM-BII energy differences between the major and minor TSs were divided into the B3LYP quantum energy of the small model part and the MM energy. With the electrostatic contribution ignored in the MM3 force field, the MM energy here consists solely of the van der Waals interaction, a long-range weak attraction, and the short-range steric repulsion. The MM contribution is further divided into the pairwise contributions between substituent groups; we call the Set 1 atoms in Figure 1 partition B as group 1, and the phenyl and naphthyl groups on the binap moiety as groups 2–7 (Figure 10).[57] For the oxidative-addition TSs, which have IMOMM differences of 6.4 kJ mol^{-1}, 3.3 kJ mol^{-1} comes from the difference in the QM energy and 3.1 kJ mol^{-1} comes from the MM energy; both the QM and MM energies contribute nearly equally to the preference of **TSo1M**. For the insertion TSs, the IMOMM difference of 4.6 kJ mol^{-1} is attributed to −1.5 kJ mol^{-1} of QM and 6.1 kJ mol^{-1} of MM energy, which is mainly steric repulsion. The QM energy favors the minor TS **TSi1m**, whereas the MM steric repulsion makes the decisive contribution that

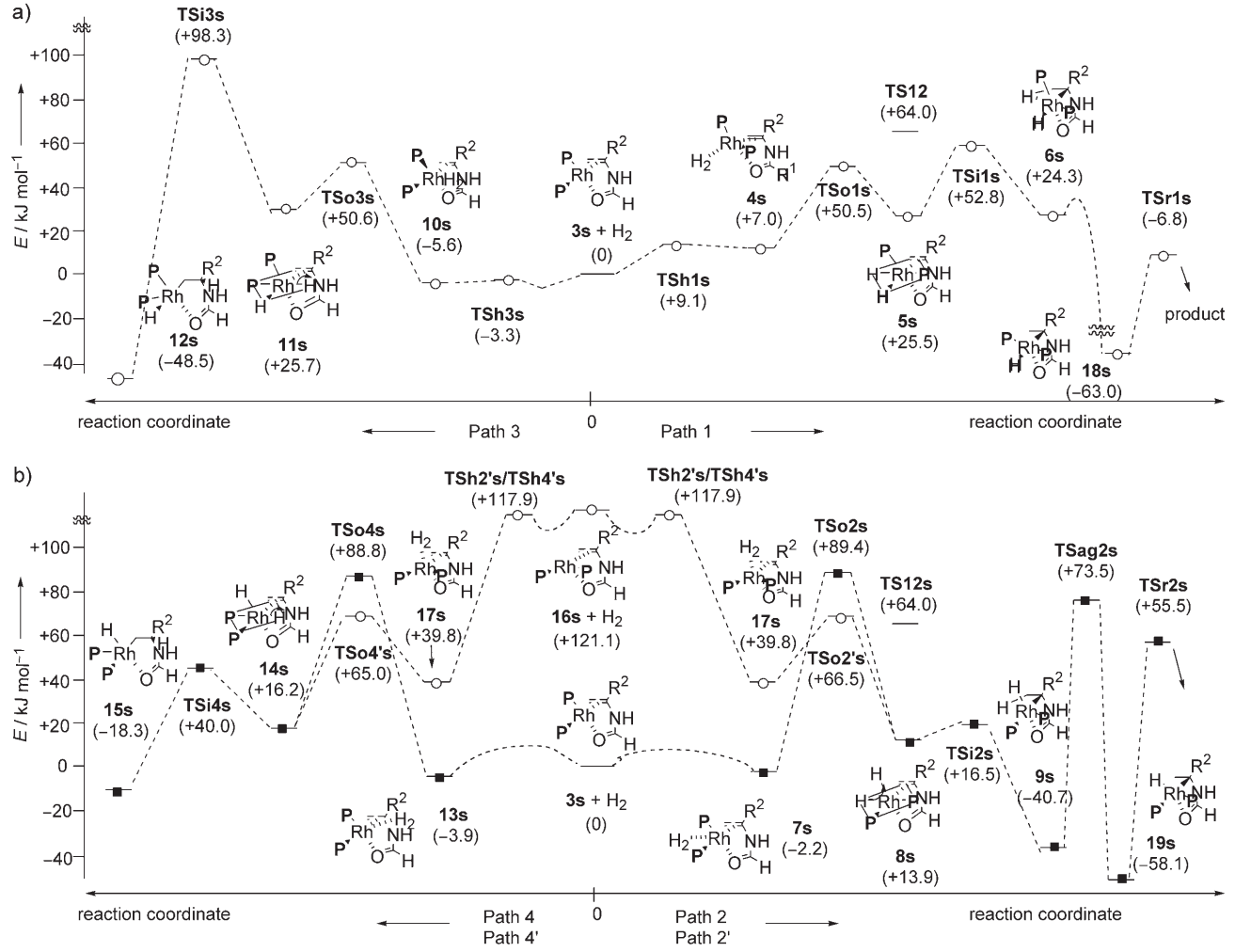

Figure 7. Energetics of the small model system optimized at the B3LYP/II level in a) Paths 1 and 3 and b) Paths 2, 2′, 4, and 4′. Energies are shown in kJ mol^{-1} relative to **3s**+H_2. R^2 = COOH. The 3-alkyl group on (*E*)-enamide is omitted for clarity.

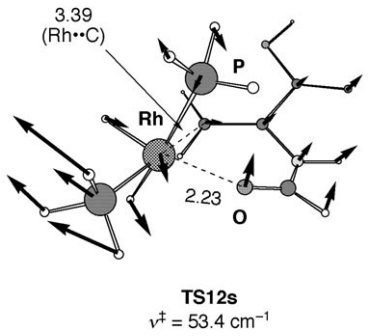

Figure 8. Structure of **TS12s** at the B3LYP/II level. Arrows are for the vibrational mode of the imaginary frequency.

favors the major TS **TSi1M**, thus overshadowing the QM contribution. Of the MM steric-repulsion contributions, the interaction between group 3 (a phenyl group on a phosphorus atom of binap) and group 5 (a naphthyl group on the other phosphorus atom of binap) makes the largest contribution of 3.9 kJ mol^{-1}, followed by many other pairs, including the groups 6 and 7 (two phenyl groups on the same phosphorus) pair of 2.4 kJ mol^{-1} and the groups 1 (the atoms in the small model system in partition B) and 7 pair of 2.3 kJ mol^{-1}. **TSi1m** has more steric repulsion than **TSi1M**.

Let us now examine Paths 2 and 2′. There could be two dihydrogen oxidative-addition TSs for each of **TSo2** and **TSo2′** in the model system. We found that in the real model system both **TSo2M** and **TSo2m** are much higher in energy than **TSo2′M** and **TSo2′m**, respectively (Figure 11). This trend in the real system is stronger than that in the model system. Therefore, in the real model system, we consider only two diastereomeric TSs, **TSo2′M** and **TSo2′m**, in Path 2′. **TSo2′M** is 3.2 kJ mol^{-1} lower in energy than **TSo2′m**. In the next step, the alkene insertion, we also found two diastereomeric TSs, **TSi2′M** and **TSi2′m**, with **TSi2M** lying 4.0 kJ mol^{-1} lower in energy than **TSi2m**. Thus, the energetics of both the oxidative-addition and alkene-insertion TSs in Paths 2 and 2′ are consistent with the experimental enantioselectivity. If the enantioselective hydrogenation occurs through Path 2, the oxidative-addition step (with higher TS energy than the insertion step) should be rate-determining,

CHEMISTRY
AN ASIAN JOURNAL

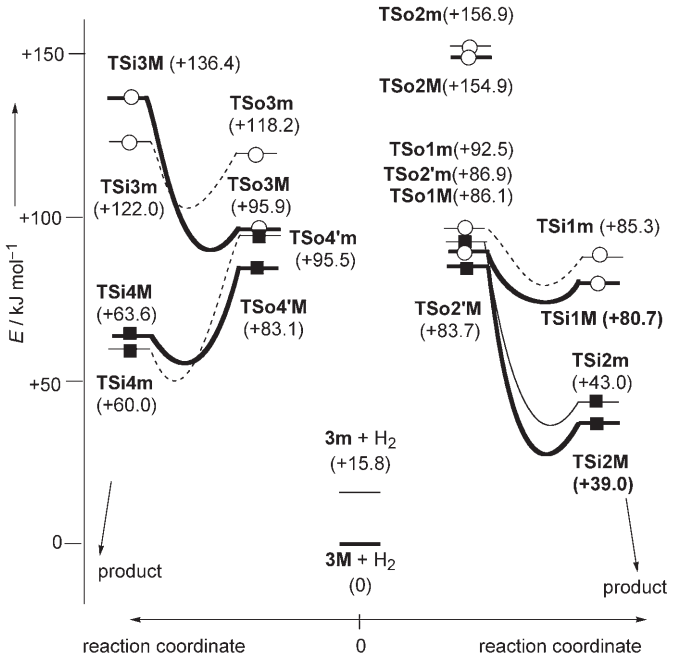

Figure 9. Energetics of the real model system at the IMOMM-BII// IMOMM-AI level. Energies are shown in kJ mol^{-1} relative to **3M**.

but both steps can contribute significantly to the enantioselectivity (with a small **m**-**M** energy difference of 3.2 kJ mol^{-1} for oxidative addition and 4.0 kJ mol^{-1} for insertion). The oxidative-addition TS **TSo2′M** is 44.7 kJ mol^{-1} higher in energy than the insertion TS **TSi2M. TSo2′M** is favored over **TSo2′m** mainly because of the favorable MM contribution; the steric repulsion is smaller in **TSo2′M** than in **TSo2′m**. On the other hand, **TSi2′M** is favored over **TSi2′m** mainly because of the favorable QM contribution; the QM part is less distorted in **TSi2′M** than in **TSi2′m**.

Overall, the lowest transition state in Paths 2 and 2′ seems to be favored over that in Path 1 in both the oxidation and the insertion step. It is, however, more likely that the reaction would proceed through Path 1 if there were no equilibrium between precursor complexes. To take the low-energy Path 2′ (through **TSo2′M** or **TSo2′m**), the reaction has to go through a very high-energy precursor dihydrogen complex **17**. Path 2 (through **TSo2M** or **TSo2m**), from the low-energy dihydrogen complex **7**, involves a very high barrier at **TSo2M** (or **m**). As discussed earlier and in previous theoretical studies,[21] a rapid equilibrium between Paths 1, 2, and 2′ through Rh dihydride complexes is likely to take place. Therefore, Paths 2 and 2′ cannot be ruled out.

Paths 3 and 4

Let us now examine the regioisomeric pathways. The bulkiness of a phenyl group in an enamide will affect the energy difference between regioisomeric pathways. In Path 3, **TSo3M** is 22.2 kJ mol^{-1} lower in energy than **TSi3m**, thus strongly favoring the major product, in agreement with experiment. On the other hand, **TSi3M** is 14.5 kJ mol^{-1} higher in energy than **TSi3m**, thus showing the opposite sense of

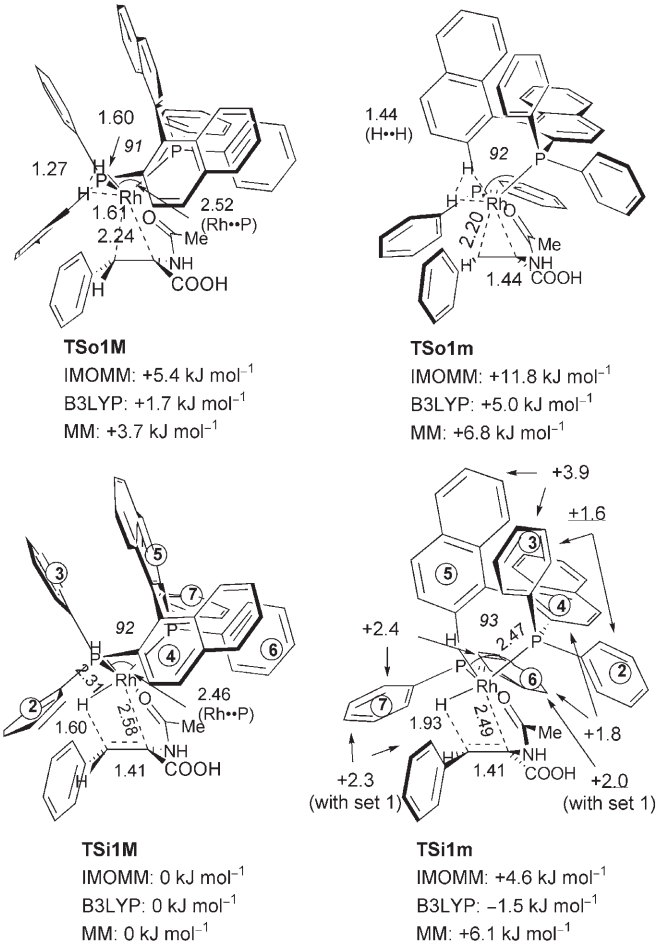

Figure 10. Structures of transition states of oxidative addition and insertion in Path 1 for the real model system at the IMOMM-AI level, with bond lengths in Å and bond angles (italics) in degrees. The IMOMM-BII energy differences between the major and minor TSs are divided into the B3LYP quantum energy of the model part and the MM energy. The MM energy is further divided into the contributions between particular groups (in parentheses).

experimental enantioselectivity (Figure 12). The situation is similar in Path 4. **TSo4′M** is 12.3 kJ mol^{-1} lower in energy than **TSo4′m**, thus strongly favoring the major product, whereas **TSi4′M** is 3.6 kJ mol^{-1} higher in energy than **TSi4′m** (Figure 13). The high energies of Paths 3 and 4 compared with Paths 1 or 2 suggest that these regioisomeric pathways are not favorable.

Conclusions

According to the current IMOMM results for the hydrogenation of enamides with a binap–Rh^{I} catalyst, the energy differences in Path 1 between the transition states for major and minor products for both the oxidative-addition and insertion steps are consistent with the experimental enantioselectivity, thus suggesting that both steps can determine the enantioselectivity when the reaction takes place by Path 1 (Scheme 2). There the oxidative addition (with higher TS

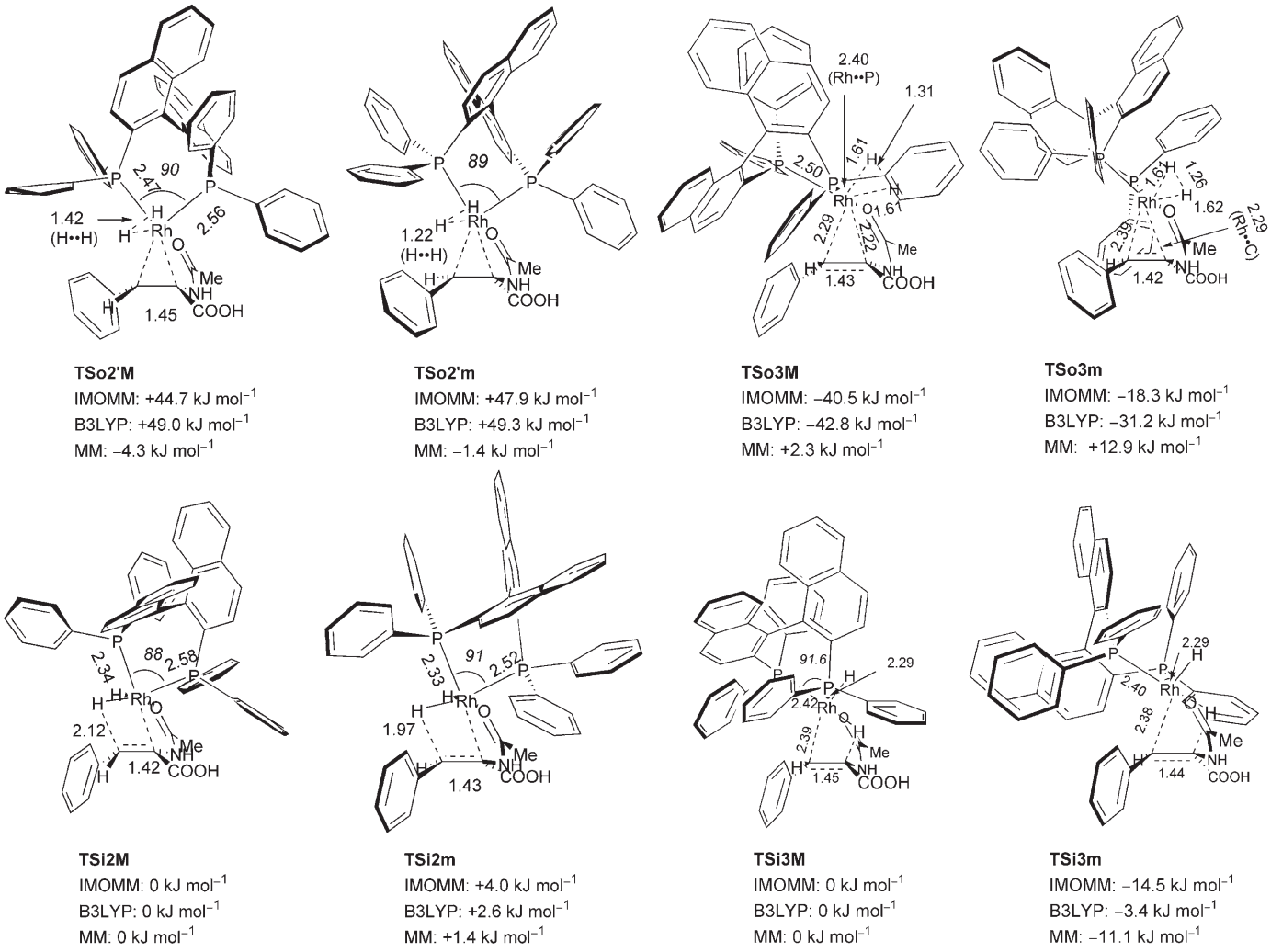

Figure 11. Structures and energies of transition states of oxidative addition and insertion in Path 2 for the real model system at the IMOMM-BII//IMOMM-AI level. See Figure 10 for details.

Figure 12. Structures and energies of transition states of oxidative addition and insertion in Path 3 of the real model system at the IMOMM-BII//IMOMM-AI level. See Figure 10 for details.

energy than the insertion step) should be rate-determining and is likely to make a larger contribution to enantioselectivity than the insertion step (with an **m**-**M** energy difference of 6.4 kJ mol^{-1} for the oxidative-addition vs. 4.6 kJ mol^{-1} for the insertion TS), although the **m**-**M** energy difference is too small for quantitative comparison. For the oxidative-addition TSs, both the QM and MM energies contribute nearly equally to the preference of **TSo1M**. For the insertion TSs, the preference of the major TS **TSi1M** is dominated by the MM energy, in particular, steric energy; the steric repulsion between the naphthyl group on one of the phosphorus atoms and the phenyl group on the other phosphorus atom in the TS makes the largest contribution.

For Paths 2 and 2′, a similar sense of enantioselectivity that is consistent with experiment is found.

If there is a rapid equilibrium between precursor dihydrogen complexes, a high barrier can be avoided, and Path 2 may become more favorable than Path 1. According to the recent experimental studies on rapid equilibria between rhodium(III) dihydride intermediates,[58] the insertion step can determine the enantioselectivity because the latter depends on H_2 pressure, as found in the case of 1,2-bis[(*o*-methoxyphenyl)phenylphosphino]ethane (dipamp).[59] Although the conformation of the observed dihydride intermediates can be proposed as **8** in Path 2 (Scheme 2) by para-hydrogen-induced polarization NMR spectroscopy,[28,56] Path 1 would be unobservable. With the present binap ligand, there also exists the possibility of an equilibrium between dihydrides, which is a subject for future study.

Notably, we found that the "lock-and-key" motif, in which the more-stable intermediate corresponds to the more-stable TS, is followed in the binap–Rh^{I}-catalyzed hydrogenation reaction as in many enzymatic reactions,[60] whereas the "anti-lock-and-key" motif is observed in the Me-duphos–Rh^{I}-catalyzed reaction.[10] Hydrogenation of α-acylaminoacrylates in the presence of [Rh((*S*,*S*)-dipamp)]$^{+}$ follows the "lock-and-key" motif.[61] The present calculation suggests that both motifs may be realized, and that in the end the

CHEMISTRY
AN ASIAN JOURNAL

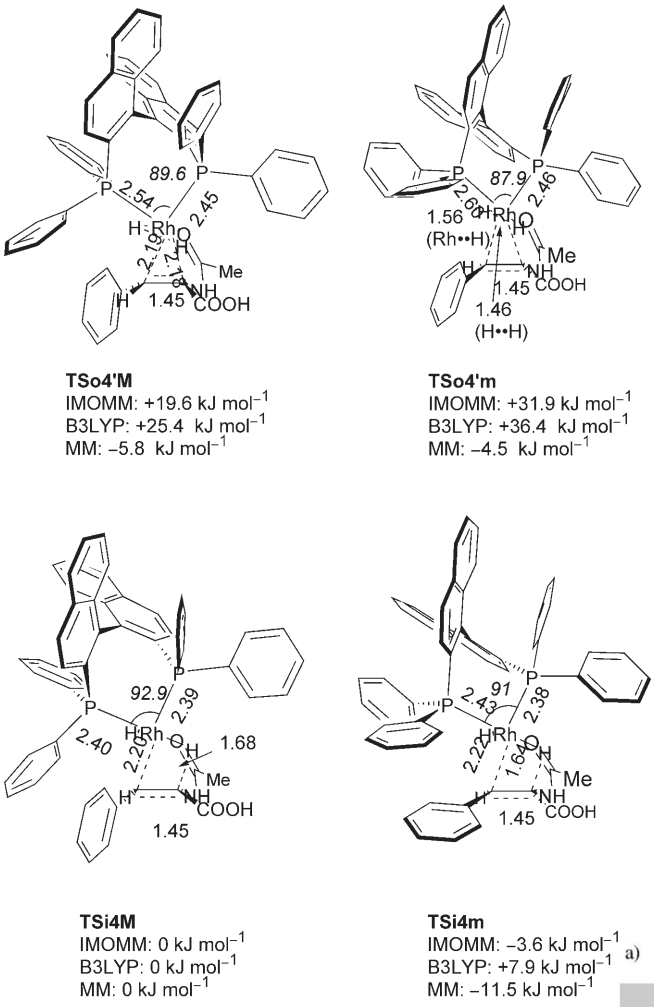

TSo4'M
IMOMM: +19.6 kJ mol^{-1}
B3LYP: +25.4 kJ mol^{-1}
MM: –5.8 kJ mol^{-1}

TSo4'm
IMOMM: +31.9 kJ mol^{-1}
B3LYP: +36.4 kJ mol^{-1}
MM: –4.5 kJ mol^{-1}

TSi4M
IMOMM: 0 kJ mol^{-1}
B3LYP: 0 kJ mol^{-1}
MM: 0 kJ mol^{-1}

TSi4m
IMOMM: –3.6 kJ mol^{-1}
B3LYP: +7.9 kJ mol^{-1}
MM: –11.5 kJ mol^{-1}

Figure 13. Structures and energies of transition states of oxidative addition and insertion in Path 4 of the real model system at the IMOMM-BII//IMOMM-AI level. See Figure 10 for details.

issue of the "lock-and-key" or "anti-lock-and-key" motif may not be very important in the step that determines the enantioselectivity.

The higher stability of **3M** over **3m** can be explained by a quadrant diagram proposed by Knowles (Figure 14).[1b] Whereas the 3-phenyl group in 2-acetylamino-3-phenylacrylic acid is far from the equatorial phenyl group on the binap ligand in **3M**, it is closer to the equatorial phenyl group in **3m**. Note that a hydrogen atom is modeled instead of the 3-phenyl group in the previous studies by Landis and Feldgus.[22] In the case of the Rh^{I}–chiraphos catalyst, the minor complex (**3cm**) is more stable than the major (**3cM**). The 3-phenyl group of the enamide in the minor complex is tilted more into an unhindered quadrant in the chiraphos case. The steric repulsion between an equatorial phenyl group on the binap ligand and the 3-phenyl group is decreased in the minor complex relative to **3m** in the Rh^{I}–binap system. The methyl group of the acetylamino group in the less stable **3m** is in a hindered quadrant. This suggests that a bulkier group such as phenyl may give higher enantioselectivity as shown by experiment ([Eq. (1)]; 84% *ee* for R^{1} = Me to 96% *ee* for R^{1} = Ph).

Further experiments as well as theoretical studies may be needed for a better understanding of the relationship between the conformations of the intermediate complexes and transition states that determine the stereoselectivity.

The experimental and computational studies on the effects of chiral ligands will be very useful for chiral technology. Although the schematic quadrant diagram is frequently used to explain the stereoselectivity, the transition states of oxidative addition and/or insertion should be used for more quantitative prediction. Investigations of the potential-energy surface of all the steps of the Rh^{I}–binap-catalyzed reaction[62] and the stereoelectronic effects of chiral ligands are currently in progress.

Computational Methods

Calculations were performed with our own IMOMM code, which combined the MM3(92) program[45] with Gaussian 98.[46] The B3LYP density functional method was used for the MO part. The basis set I consisted of LANL2DZ basis functions, which included a double-zeta valence basis set (8 s5p5d)/[3s3p2d] with the Hay and Wadt effective core potential (ECP)[47] replacing core electrons up to 3p for the Rh atom and the Huzinaga–Dunning valence double-zeta quality basis set[48] for the remaining atoms, supplemented with a set of d functions ($\alpha = 0.387$)[49] for the phos-

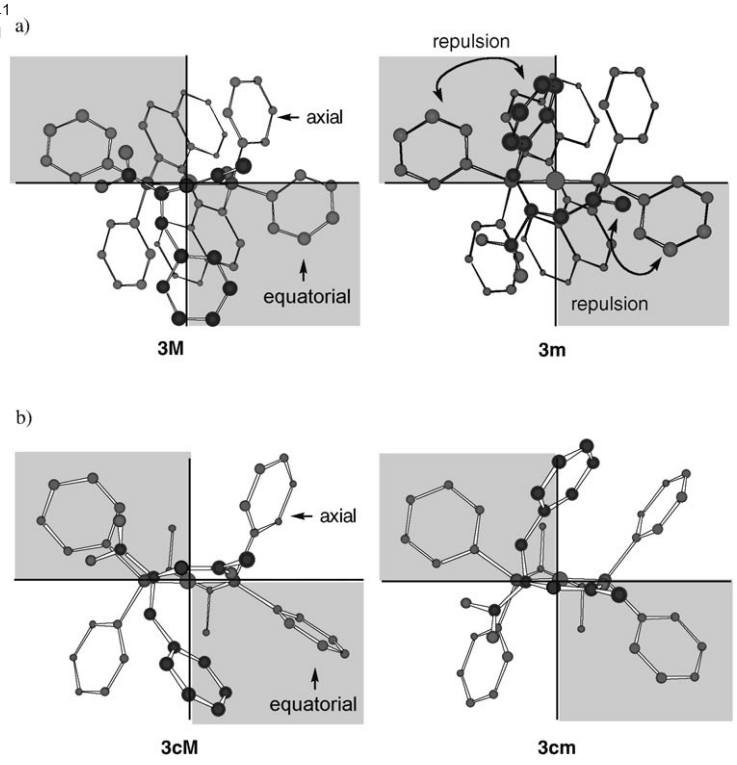

Figure 14. Quadrant diagrams of a) Rh^{I}–(*R*)-binap and b) Rh^{I}–(*S*,*S*)-chiraphos complexes with 2-acetylamino-3-phenylacrylic acid at the IMOMM-AI level. Hindered quadrants are shown shaded.

phorus atom. Although the effects of the d functions were significant in the Rh–P bond lengths, d and p functions for the H, C, N, and O atoms did not have large effects on structures and energetics. We also used basis set II, which consisted of basis set I for Rh and P atoms and the D95* basis set for C, H, N, and O atoms. The optimized structures for $[RhH_2(PH_3)_2]$ and $CH_2=C(NHCHO)COOH$ were found to be essentially the same for B3LYP/I and /II calculations.

For Paths 1–4, we focused on the transition states of the hydrogen molecule oxidative-addition and enamide insertion steps of the reaction of **1** by using the two IMOMM partitions as shown in Figure 1. In partition A (IMOMM-A), Set 1 atoms were included in the model system, and Set 3 atoms were replaced by hydrogen atoms in the small model system. Set 1 and 3 atoms were handled with the B3LYP method. Set 4 atoms were included only in the real model system that was handled at the MM level. In partition B (IMOMM-B), the phenyl and methyl groups in 2-acetylamino-3-phenylacrylic acid and the seven-membered ring (Figure 1) of the binap ligand were included in the model part to investigate their electronic effects, whereas in partition A, they were considered in the real part only. The optimization was mostly performed without symmetry constraints by using IMOMM-A(B3LYP/I:MM3) (further abbreviated as IMOMM-AI). The energy was improved with IMOMM-B(B3LYP/II:MM3) (abbreviated as IMOMM-BII); even in this case in which the geometry of the quantum mechanics (QM) part was frozen, the MM part was reoptimized. The nature of stationary points was characterized based on the normal coordinate analysis of the small model part, and the eigenvector corresponding to the only negative eigenvalue of every transition state was visually checked to confirm its connectivity with the reactant and product of the step. The fixed linked bond lengths were r(P–H) = 1.42 Å, r(C(olefin)–C(phenyl)) = 1.51 Å, r(P–Ar) = 1.84 Å, r(C(olefin)–H) = 1.096 Å, r(C(amide)–H) = 1.02 Å, r(C(amide)–Me) = 1.51 Å, and r(P–Ar) = 1.84 Å. IMOMM-BII optimized geometries were found to be very similar to the IMOMM-AI geometries, although their energies were somewhat different in some cases (see Supporting Information for more details of IMOMM-BII vs. IMOMM-AI).

The MM3(92) force field was used for the MM part of the remaining system (Figure 1). The MM3 force field is widely used for organometallic systems and exhibits smaller average errors than UFF (Universal Force Field).[50,51] Pariser–Parr–Pople type SCF (self-consistent field) corrections were applied to the MM3 force field, because the delocalization effects of the binap moiety should be considered.[52] The UFF van der Waals parameters by Rappé et al.[53] were used for the Rh atom, while all other MM contributions involving the metal atom were set to zero; this is not a bad approximation, since the metal MM parameter was used only for the interaction of the QM and MM parts, which are mutually separated by at least one extra atom and are quite far away for any significant MM interaction to take place. The electronic effects of the (bulky) MM substituents were neglected in the IMOMM treatment.

Acknowledgements

We thank Dr. D. V. Khoroshun, Dr. S. Irle, and Dr. M. Oshima for helpful suggestions, and the Cherry L. Emerson Center of Emory University for the use of its resources. This work is supported by a grant (CHE-0209660) from the National Science Foundation to K.M. and by a grant from the Mitsubishi Chemical Corporation Fund to S.M. Generous allotment of computational time from the National Center for Supercomputing Applications, Illinois, the Maui High-Performance Computer Center, Hawaii, and from the Institute for Molecular Science, Okazaki (Japan) is gratefully acknowledged.

[1] a) W. S. Knowles, M. J. Sabacky, *Chem. Commun. (London)* **1968**, 1445–1446; b) W. S. Knowles, *Acc. Chem. Res.* **1983**, *16*, 106–112; c) W. S. Knowles, *Angew. Chem.* **2002**, *114*, 2096–2107; *Angew. Chem. Int. Ed.* **2002**, *41*, 1998–2007.

[2] a) T. P. Dang, H. B. Kagan, *J. Chem. Soc. Chem. Commun.* **1971**, 481; b) H. B. Kagan, N. Langlois, T. P. Dang, *J. Organomet. Chem.* **1975**, *90*, 353.

[3] a) A. Miyashita, A. Yasuda, H. Takaya, K. Toriumi, T. Ito, T. Souchi, R. Noyori, *J. Am. Chem. Soc.* **1980**, *102*, 7932–7934; b) R. Noyori, M. Ohta, Y. Hisao, M. Kitamura, T. Ohta, H. Takaya, *J. Am. Chem. Soc.* **1986**, *108*, 7117–7119; c) R. Noyori, *Angew. Chem.* **2002**, *114*, 2108–2123; *Angew. Chem. Int. Ed.* **2002**, *41*, 2008–2022.

[4] Reviews: a) H. Takaya, T. Ohta, R. Noyori in *Catalytic Asymmetric Synthesis, 2nd ed.* (Ed.: I. Ojima), Wiley-VCH, Weinheim, **2000**, chap. 1; b) R. A. Sánchez-Delgado, M. Rosales, *Coord. Chem. Rev.* **2000**, *196*, 249–280; c) M. J. Burk, *Acc. Chem. Res.* **2000**, *33*, 363–372; d) M. Tsukamoto, M. Kitamura, *Yuki Gosei Kagaku Shi (J. Syn. Org. Jpn.)* **2005**, *63*, 899–910.

[5] Examples: G. Zhu, P. Cao, Q. Jiang, X. Zhang, *J. Am. Chem. Soc.* **1997**, *119*, 1799–1800.

[6] Review: I. D. Gridnev, T. Imamoto, *Acc. Chem. Res.* **2004**, *37*, 633–644.

[7] C. R. Landis, T. W. Brauch, *Inorg. Chim. Acta* **1998**, *270*, 285–297.

[8] a) J. M. Brown, *Chem. Soc. Rev.* **1993**, *22*, 25–41; b) J. M. Brown, *J. Organomet. Chem.* **2004**, *689*, 4006–4015.

[9] J. M. Brown, P. A. Chaloner, *J. Chem. Soc. Chem. Commun.* **1980**, 344–346.

[10] C. R. Landis, J. Halpern, *J. Am. Chem. Soc.* **1987**, *109*, 1746–1754.

[11] I. D. Gridnev, T. Imamoto, *Acc. Chem. Res.* **2004**, *37*, 633–643.

[12] A. S. C. Chan, J. J. Pluth, J. Halpern, *J. Am. Chem. Soc.* **1980**, *102*, 5952–5954.

[13] B. McCulloch, J. Halpern, M. R. Thompson, C. R. Landis, *Organometallics* **1990**, *9*, 1392–1395.

[14] P. S. Chua, N. K. Roberts, B. Bosnich, S. J. Okrasinsi, J. Halpern, *J. Chem. Soc. Chem. Commun.* **1981**, 1278–1981.

[15] *Mechanisms in Homogeneous Catalysis: A Spectroscopic Approach* (Ed.: B. Heaton), Wiley-VCH, Weinhelm, **2005**.

[16] B. R. Bender, M. Koller, D. Nanz, W. von Philipsborn, *J. Am. Chem. Soc.* **1993**, *115*, 5889–5890.

[17] M. S. Chinn, R. Eisenberg, *J. Am. Chem. Soc.* **1992**, *114*, 1908–1909.

[18] T. Schmidt, W. Baumann, H.-J. Drexler, A. Arrieta, D. Heller, H. Buschmann, *Organometallics* **2005**, *24*, 3842–3848.

[19] Previous theoretical studies on the potential-energy profile of the ethylene hydrogenation of Rh^I catalysts: C. Daniel, N. Koga, J. Han, X. Y. Fu, K. Morokuma, *J. Am. Chem. Soc.* **1988**, *110*, 3773–3787.

[20] Previous theoretical studies concerned the geometries of [Rh(diphosphine)(olefin)] complexes. Molecular graphics studies: a) J. M. Brown, P. L. Evans, *Tetrahedron* **1988**, *44*, 4905–4916; b) P. L. Bogdan, J. J. Irwin, B. Bosnich, *Organometallics* **1989**, *8*, 1450–1453.

[21] C. R. Landis, S. Feldgus, *J. Am. Chem. Soc.* **1999**, *121*, 8741–8754.

[22] a) C. R. Landis, S. Feldgus, *Angew. Chem.* **2000**, *112*, 2985–2988; *Angew. Chem. Int. Ed.* **2000**, *39*, 2863–2865; b) S. Feldgus, C. R. Landis, *J. Am. Chem. Soc.* **2000**, *122*, 12714–12727; c) S. Feldgus, C. R. Landis, *Organometallics* **2001**, *20*, 2374–2386; d) M. Li, D. Tang, X. Luo, W. Shen, *Int. J. Quantum Chem.* **2005**, *102*, 53–63.

[23] A. Kles, A. Börner, D. Heller, R. Selke, *Organometallics* **1997**, *16*, 2096–2100.

[24] J. S. Glovannetti, C. M. Kelly, C. R. Landis, *J. Am. Chem. Soc.* **1993**, *115*, 4040–4057.

[25] a) J. M. Brown, P. A. Chaloner, G. A. Morris, *J. Chem. Soc. Perkin Trans. 2* **1987**, 1583–1588; b) J. M. Brown, J. A. Ramsden, J. M. Claridge, *J. Chem. Soc. Chem. Commun.* **1995**, 2469–2471; c) B. R. Bender, M. Koller, D. Nanz, W. von Philipsborn, *J. Am. Chem. Soc.* **1993**, *115*, 5889–5890.

[26] I. Ojima, T. Kogure, N. Yoda, *J. Org. Chem.* **1980**, *45*, 4728–4739.

[27] D. Sinou, *Tetrahedron Lett.* **1981**, *22*, 2987–2990.

[28] A. Harthun, R. Kadyrov, R. Selke, J. Bargon, *Angew. Chem.* **1997**, *109*, 1155–1156; *Angew. Chem. Int. Ed. Engl.* **1997**, *36*, 1103–1105.

[29] a) M. M. Taqui Khan, S. A. Samad, M. R. H. Siddiqui, *J. Mol. Catal.* **1989**, *53*, 23; b) M. M. Taqui Khan, B. Taqui Khan, S. M. Ali, *J. Mol. Catal.* **1989**, *57*, 29 and references cited therein.

[30] I. D. Gridnev, M. Yasutake, N. Higashi, T. Imamoto, *J. Am. Chem. Soc.* **2001**, *123*, 5268–5276.
[31] I. D. Gridnev, Y. Yamanoi, N. Higashi, H. Tsuruka, M. Yasutake, T. Imamoto, *Adv. Synth. Catal.* **2001**, *343*, 118–136.
[32] R. Giernoth, H. Heinrich, N. J. Adams, R. J. Deeth, J. Bargon, J. M. Brown, *J. Am. Chem. Soc.* **2000**, *122*, 12381–12382.
[33] I. D. Gridnev, M. Yasutake, T. Imamoto, I. P. Beletskaya, *Proc. Natl. Acad. Sci. USA* **2004**, *101*, 5385–5390.
[34] A. Miyashita, H. Takaya, T. Souchi, R. Noyori, *Tetrahedron* **1984**, *40*, 1245–1253.
[35] M. Kitamura, M. Tsukamoto, Y. Bessho, M. Yoshimura, U. M. Kobs, Widhalm, R. Noyori, *J. Am. Chem. Soc.* **2002**, *124*, 6649–6667.
[36] B. F. M. Kimmich, E. Somsook, C. R. Landis, *J. Am. Chem. Soc.* **1998**, *120*, 10115–10125.
[37] There are two conformational isomers with respect to the COOH moiety but we showed just one. Except for the COOH moieties, transition structures and energetics are essentially the same in the model reaction system.
[38] C. R. Landis, P. Hilfenhaus, S. Feldgus, *J. Am. Chem. Soc.* **1999**, *121*, 8741–8754.
[39] D. W. Price, M. G. B. Drew, K. K. M. Hii, J. M. Brown, *Chem. Eur. J.* **2000**, *6*, 4587–4596.
[40] a) F. Maseras, *Computational Organometallic Chemistry* (Ed.: T. R. Cundari), Marcel Dekker, New York, **2001**, pp. 159–183; b) G. Ujaque, F. Maseras in *Principles and Applications of Density Functional Theory in Inorganic Chemistry I* (Eds.: N. Kaltsoyannis and J. E. McGrady), Springer, Heidelberg, **2004**, pp. 117–150.
[41] a) R. Schmid, W. A. Hermann, G. Frenking, *Organometallics* **1997**, *16*, 701–708; b) D. Gleich, J. Hutter, *Chem. Eur. J.* **2004**, *10*, 2435–2444.
[42] F. Maseras, K. Morokuma, *J. Comput. Chem.* **1995**, *16*, 1170–1179.
[43] a) T. Matsubara, F. Maseras, N. Koga, K. Morokuma, *J. Phys. Chem.* **1996**, *100*, 2573–2580; b) D. G. Musaev, R. D. J. Froese, K. Morokuma, *Organometallics* **1998**, *17*, 1850–1860; c) D. V. Khoroshun, D. G. Musaev, T. Vreven, K. Morokuma, *Organometallics* **2001**, *20*, 2007–2026; d) G. Ujaque, F. Maseras, A. Lledós, *J. Am. Chem. Soc.* **1999**, *121*, 1317–1323; e) J. J. Carbo, F. Maseras, C. Bo, P. W. N. M. van Leeuwen, *J. Am. Chem. Soc.* **2001**, *123*, 7630–7637; f) D. V. Khoroshun, D. G. Musaev, T. Vreven, K. Morokuma, *Organometallics* **2001**, *20*, 2007–2026; g) M. Torrent, T. Vreven, D. G. Musaev, K. Morokuma, *J. Am. Chem. Soc.* **2002**, *124*, 192–193; h) E. Daura-Oller, A. M. Segarra, J. M. Poblet, C. Claver, E. Fernández, C. Bo, *J. Org. Chem.* **2004**, *69*, 2669–2680; i) G. Ujaque, F. Maseras, *Structure and Bonding* **2004**, *112*, 117–149; j) D. Balcells, F. Maseras, G. Ujaque, *J. Am. Chem. Soc.* **2005**, *127*, 3624–3634.
[44] a) M. Svensson, S. Humbel, R. D. J. Froese, T. Matsubara, S. Sieber, K. Morokuma, *J. Phys. Chem.* **1996**, *100*, 19357; b) S. Dapprich, I. Komáromi, K. S. Byun, K. Morokuma, M. J. Frisch, *THEOCHEM* **1999**, *461–462*, 1–21; c) T. Vreven, K. Morokuma, *J. Comput. Chem.* **2000**, *21*, 1419; d) T. Vreven, K. Morokuma, Ö. Farkas, H. B. Schlegel, M. J. Frisch, *J. Comput. Chem.* **2003**, *24*, 760–769.
[45] N. L. Allinger, *MM3(92)*, Indiana University, Bloomington (USA), **1992**.
[46] Gaussian 98 (Revision A.7): M. J. Frisch, G. W. Trucks, H. B. Schlegel, G. E. Scuseria, M. A. Robb, J. R. Cheeseman, V. G. Zakrevski, J. A. Montgomery, R. E. Stratmann, J. C. Burant, S. Dapprich, J. M. Millam, A. D. Daniels, K. N. Kudin, M. C. Strain, O. Farkas, J. Tomasi, V. Barone, M. Cossi, R. Cammi, B. Mennucci, C. Pomelli, A. Adamo, S. Clifford, J. Ochterski, G. A. Petersson, P. Y. Ayala, Q. Cui, K. Morokuma, D. K. Malick, A. D. Rabuck, K. Raghavachari, J. B. Foersman, J. Cioslowski, J. V. Ortiz, B. Stefanov, G. Liu, A. Liashenko, P. Piskorz, I. Komaromi, R. Gomperts, M. L. Martin, D. J. Fox, T. Keith, M. A. Al-Laham, C. Y. Peng, A. Nanayakkara, C. Gonzalez, M. Challacombe, P. M. W. Gill, B. G. Johnson, W. Chen, M. W. Wong, J. L. Andres, M. Head-Gordon, E. S. Replogle, J. A. Pople, Gaussian, Inc., Pittsburgh (USA), **1998**.
[47] P. J. Hay, W. R. Wadt, *J. Chem. Phys.* **1985**, *82*, 299–310.
[48] a) T. M. Dunning, Jr., *J. Chem. Phys.* **1971**, *55*, 716–723; b) T. M. Dunning, Jr., *J. Chem. Phys.* **1970**, *53*, 2823–2833.
[49] A. Höllwarth, M. Böhme, S. Dapprich, A. W. Ehlers, A. Gobbi, V. Jonas, K. F. Köhler, R. Stegmann, A. Veldkamp, G. Frenking, *Chem. Phys. Lett.* **1993**, *208*, 237–240.
[50] a) H. Hagelin, M. Svensson, B. Åkermark, P.-O. Norrby, *Organometallics* **1999**, *18*, 4574–4583; b) H. Hagelin, B. Åkermark, P.-O. Norrby, *Organometallics* **1999**, *18*, 2884–2895.
[51] I. Petterson, T. Liljefors in *Reviews in Computational Chemistry, Vol. 9* (Eds.: K. B. Lipkowitz, D. B. Boyd), VCH, New York, **1996**, pp. 167–189.
[52] J. T. Sprague, J. C. Tai, Y. Yuh, N. L. Allinger, *J. Comput. Chem.* **1987**, *8*, 581–603.
[53] A. K. Rappé, C. J. Casewit, K. S. Colwell, W. A. Goddard III, W. M. Skiff, *J. Am. Chem. Soc.* **1992**, *114*, 10024–10035.
[54] A. S. C. Chan, J. J. Pluth, J. Halpern, *Inorg. Chim. Acta* **1979**, *37*, L477–L779.
[55] A. S. C. Chan, J. Halpern, *J. Am. Chem. Soc.* **1980**. *102*, 838–840.
[56] H. Heinrich, R. Giernoth, J. Bergon, J. M. Brown, *Chem. Commun.* **2001**, 1296–1297.
[57] Details of partitions of MM3 energies into terms are described elsewhere; see reference [3d].
[58] I. D. Gridnev, N. Higashi, K. Asakura, T. Imamoto, *J. Am. Chem. Soc.* **2000**, *122*, 7183–7194.
[59] J. M. Brown, P. A. Chaloner, *J. Chem. Soc. Chem. Commun.* **1978**, 321–322.
[60] A. Fersht, *Structure and Mechanism in Protein Science*, W. H. Freeman, New York, **1999**.
[61] a) H.-J. Drexler, W. Baumann, T. Schmidt, S. Zhang, A. Sun, A. Spannenberg, C. Fischer, H. Buschmann, D. Heller, *Angew. Chem.* **2005**, *117*, 1208–1212; *Angew. Chem. Int. Ed.* **2005**, *44*, 1184–1188; b) D. A. Evans, F. E. Michael, J. S. Tedrow, K. R. Campos, *J. Am. Chem. Soc.* **2003**, *125*, 3534–3543; c) M. T. Reetz, A. Meiswinkel, G. Mehler, K. Amgermund, M. Graf, W. Thiel, R. Mynott, D. G. Blackmond, *J. Am. Chem. Soc.* **2005**, *127*, 10305–10313.
[62] Several Rh^{III} dihydride complexes cannot be located by IMOMM methods and led to the dissociation between rhodium and olefin. This is because we could treat only the steric effects and not the electronic effects of substituents in the real system at the level of the method, and because a microiteration protocol was used on the current version of the IMOMM program. A more appropriate method would be an optimization with the full gradient and Hessian matrix as adopted in a recent implementation of the ONIOM method; see: T. Vreven, M. J. Frisch, K. N. Kudin, H. B. Schlegel, K. Morokuma, *Mol. Phys.* **2006**, 104, 701–714; see also reference [44d].

Received: February 3, 2006
Published online: August 17, 2006

